Formation of Porous Aluminophosphate Frameworks Monitored by Hyperpolarized ^{129}Xe NMR Spectroscopy

Devin N. Sears,[†] Bryan A. Demko,[†] Kristopher J. Ooms,[†] Roderick E. Wasylishen,*[,†] and Yining Huang[‡]

Department of Chemistry, University of Alberta, Edmonton, Alberta, T6G 2G2 Canada, and Department of Chemistry, University of Western Ontario, London, Ontario, N6A 5B8 Canada

Received June 18, 2005. Revised Manuscript Received August 1, 2005

The formation of two aluminophosphate frameworks, $AlPO_4$-5 and $AlPO_4$-18, has been monitored using hyperpolarized ^{129}Xe NMR as a probe. The reaction progress from an amorphous phase to $AlPO_4$-5 and its subsequent conversion to $AlPO_4$-18 is observed for xenon adsorbed in samples that have been reacted for varying lengths of time. The extreme sensitivity of ^{129}Xe chemical shifts to local environments of the xenon leads to separate NMR peaks for xenon adsorbed in the two different aluminophosphate frameworks present in a single reaction mixture. For xenon adsorbed in $AlPO_4$-5, an anisotropic ^{129}Xe NMR line shape at $\delta_{iso} \approx 63$ ppm is observed, whereas for xenon in $AlPO_4$-18, a peak with a small anisotropy at $\delta_{iso} \approx 74$ ppm is observed. Grand canonical Monte Carlo simulations provide a theoretical description of xenon adsorbed in the two aluminophosphate frameworks, and the resulting simulated ^{129}Xe NMR line shapes are in good agreement with experimental data. Two-dimensional exchange NMR spectroscopy was used to examine the exchange of xenon between $AlPO_4$-5, $AlPO_4$-18, and bulk xenon gas. The results indicate that the domains of $AlPO_4$-5 are in intimate contact with those of $AlPO_4$-18, facilitating a higher intercrystallite exchange than with the bulk xenon gas.

Introduction

Porous materials having pore dimensions between 5 and 20 Å are of interest because of their applications as molecular sieves, catalysts, or supporting frameworks in catalytic processes.[1−3] The inorganic aluminosilicates, or zeolites, are the most commonly studied microporous materials because of their well-defined framework topologies and desirable catalytic properties.[4] Techniques such as X-ray crystallography,[5−7] powder X-ray diffraction (XRD),[8−10] infrared spectroscopy (IR),[11,12] Raman spectroscopy,[13−15] and nuclear magnetic resonance spectroscopy (NMR)[16−21] have been used to characterize aluminosilicate zeolites, as well as materials adsorbed within their pores.[6,12,22] Particularly, NMR, Raman, and IR spectroscopies have been invaluable for the investigations of catalytic and separation processes that can occur when molecules are adsorbed within the pores of the aluminosilicate zeolites.[13−15,23−26]

Analogous to the 1:1 aluminosilicate zeolites, which ideally have alternating AlO_4-SiO_4 framework tetrahedra (Al−O−Si−O−Al linkages), microporous frameworks have been synthesized from aluminophosphates ($AlPO_4$) with alternating AlO_4-PO_4 framework tetrahedra (Al−O−P−O−Al linkages).[27−29] The $AlPO_4$s have been investigated for

* Corresponding author: Tel: (780) 492-4336. Fax: (780) 492-8231. E-mail: Roderick.Wasylishen@ualberta.ca.

[†] University of Alberta.

[‡] University of Western Ontario.

(1) *Shape Selective Catalysis in Industrial Applications*; Chen, N. Y., Garwood, W. E., Dwyer, F. G., Eds.; Marcel Dekker: New York, 1989.
(2) *Guidelines for Mastering the Properties of Molecular Sieves: Relationship Between Physicochemical Properties of Zeolitic Systems and Their Low Dimensionality*; Barthomeuf, D., Derouane, E. G., Holderich, W., Eds.; NATO ASI Ser. 221; Plenum: New York, 1989.
(3) *Studies in Surface Science and Catalysis, Zeolites and Related Microporous Materials: State of the Art* 1994; Weitkamp, J., Karge, H. G., Pfeifer, H., Holderich, W., Eds.; Elsevier: Amsterdam, 1994.
(4) *Handbook of Zeolite Science and Technology*; Auerbach, S. M., Carrado, K. A., Dutta, P. K., Eds.; Marcel Dekker: New York, 2003.
(5) Yanagida, R. Y.; Seff, K. *J. Phys. Chem.* **1973**, *77*, 138.
(6) Amaro, A. A.; Seff, K. *J. Phys. Chem.* **1973**, *77*, 906.
(7) van Koningsveld, H. *Acta Crystallogr.* **1990**, B*46*, 731.
(8) Breck, D. W.; Eversole, W. G.; Milton, R. M.; Reed, T. B.; Thomas, T. *J. Am. Chem. Soc.* **1956**, *78*, 5963.
(9) Pluth, J. J.; Smith, J. V. *J. Am. Chem. Soc.* **1980**, *102*, 4704.
(10) Colligan, M.; Forster, P. M.; Cheetham, A. K.; Lee, Y.; Vogt, T.; Hriljac, J. A. *J. Am. Chem. Soc.* **2004**, *126*, 12015.
(11) Barrachin, B.; Cohen de Lara, E. *J. Chem. Soc., Faraday Trans. 2* **1986**, *82*, 1953.
(12) Soussen-Jacob, J.; Goulay, A. M.; Cohen de Lara, E. *Mol. Phys.* **1992**, *76*, 1037.
(13) Huang, Y.; Qui. P. *Langmuir* **1999**, *15*, 1591.
(14) Huang, Y.; Havenga, E. A. *J. Phys. Chem. B* **2000**, *104*, 5084.
(15) Huang, Y.; Havenga, E. A. *Microporous Mesoporous Mater.* **2001**, *42*, 77.
(16) Klinowski, J. In *Solid-state NMR spectroscopy principles and applications*; Duer M. J., Ed., Blackwell: Oxford, 2002; Chapter 9.
(17) Fyfe, C. A.; Thomas, J. M.; Klinowski, J.; Gobbi, G. C. *Angew. Chem., Int. Ed. Engl.* **1983**, *22*, 257.
(18) Fyfe, C. A.; Gobbi, G. C.; Murphy, W. J.; Ozubko, R. S.; Slack, D. A. *J. Am. Chem. Soc.* **1984**, *106*, 4435.
(19) Hunger, M.; Engelhardt, G.; Koller, H.; Weitkamp, J. *Solid State Nucl. Magn. Reson.* **1993**, *2*, 111.
(20) Feuerstein, M.; Hunger, M.; Engelhardt, G.; Amoureux, J. P. *Solid State Nucl. Magn. Reson.* **1996**, *7*, 95.
(21) Fyfe, C. A.; Mueller, K. T.; Kokotailo, G. T. In *NMR Techniques in Catalysis*; Bell, A. T., Pines, A., Eds.; Marcel Dekker: New York, 1994; Chapter 1.
(22) Muha, G. M.; Yates, D. J. C. *J. Chem. Phys.* **1968**, *49*, 5073.
(23) Delaval, Y.; Seloudoux, R.; Cohen de Lara, E. *J. Chem. Soc., Faraday Trans. 1* **1986**, *82*, 365.
(24) Munson, E. J.; Haw J. F. *J. Am. Chem. Soc.* **1991**, *95*, 9420.
(25) Oliver, F. G.; Munson, E. J.; Haw, J. F. *J. Phys. Chem.* **1992**, *92*, 8106.
(26) Haw, J. F. In *NMR Techniques in Catalysis*; Bell, A. T., Pines, A., Eds.; Marcel Dekker: New York, 1994; Chapter 3.

10.1021/cm0513132 CCC: $30.25
Published on Web 10/06/2005

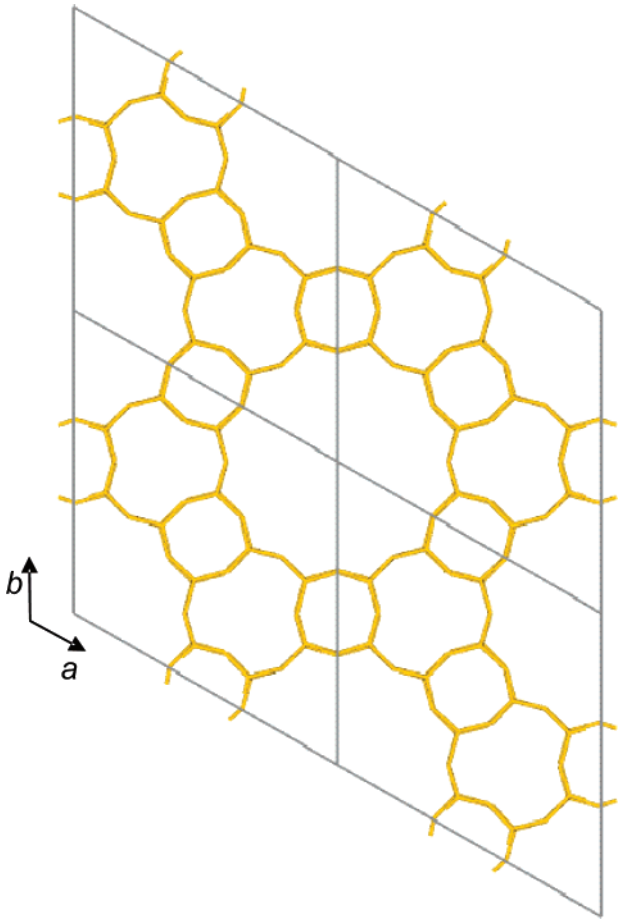

Figure 1. Skeletal structure of $AlPO_4$-5 showing the one-dimensional pores along the *c*-axis.[39] The labels *a*, *b*, and *c* represent the crystallographic axis system of the hexagonal *P*6*cc* crystal. The *ab* plane is shown to emphasize the one-dimensional channel.

applications as adsorbents, catalyst supports, and catalysts.[29,30] Some of the $AlPO_4$s have identical framework structures as the aluminosilicates; however, aluminophosphates with unique frameworks have been reported.[28] An important attribute of the $AlPO_4$s is that catalytic activity can be introduced and controlled by the introduction of silicon or metal atoms into their frameworks.[31−37] Recent studies carried out by two of the authors have followed the formation of $AlPO_4$-18 by XRD in conjunction with ^{31}P and ^{27}Al solid-state NMR.[38] The formation of $AlPO_4$-18 was shown to progress from an amorphous aluminophosphate stage to the one-dimensional porous material $AlPO_4$-5, which is finally converted to the three-dimensional pore system of $AlPO_4$-18.

The $AlPO_4$-5 channel has a diameter of approximately 7.3 Å[39] and belongs to the framework classification group AFI.[40] A view down the crystallographic *c*-axis, shown in Figure 1, clearly illustrates the one-dimension channel. The $AlPO_4$-18 framework is unique to the aluminophosphates and belongs to the AEI structural classification group.[41] As shown in Figure 2, one of the three orthogonal channels of $AlPO_4$-18 coincides with the crystallographic *c*-axis. At the intersection of the three channels is an asymmetric pear-shaped cage with approximate dimensions of 7.5 × 10.5 Å and windows approximately 3.8 Å in diameter.

The use of ^{129}Xe NMR spectroscopy has been instrumental in the characterization of the aluminosilicates, providing detailed information as to the size, shape, and local electronic structure of the micropores within their frameworks.[42−45] In addition to providing structural information, ^{129}Xe NMR has also been used to study the dynamics of xenon in porous materials.[46−48] In contrast to the aluminosilicates, relatively

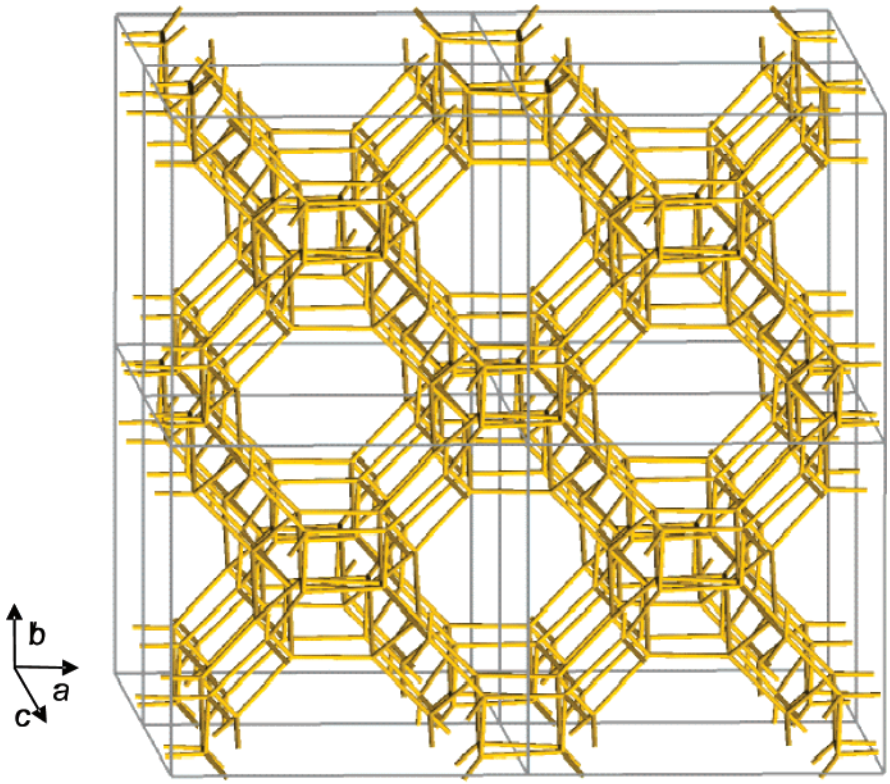

Figure 2. Skeletal structure of $AlPO_4$-18 illustrating one of the three orthogonal channels along the *c*-axis; for clarity the oxygen atoms have been omitted.[41] The labels *a*, *b*, and *c* represent the crystallographic axis system of the monoclinic *C*2/*c* crystal.

few studies have been carried out using ^{129}Xe NMR to investigate the pores of aluminophosphate frameworks[49−58] and none involving $AlPO_4$-18. In this report, we have followed the formation of $AlPO_4$-18 using hyperpolarized ^{129}Xe NMR spectroscopy to examine the reaction products of syntheses as a function of reaction time. ^{129}Xe NMR is a direct probe of the porosity of the reaction products, providing detailed information about the internal free-volume of the frameworks that XRD and solid-state ^{31}P and ^{27}Al NMR cannot.

In conjunction with the experimental results, grand canonical Monte Carlo (GCMC) simulations were carried out to aid in the interpretation of the experimental data. Finally, two-dimensional exchange NMR spectroscopy (2D-EXSY) was used to examine xenon transport between the bulk gas and the two aluminophosphate domains present at an intermediate time during the $AlPO_4$-5 to $AlPO_4$-18 conversion. This combined experimental and theoretical approach is shown to be an effective method for characterizing microporous materials at various stages of their synthetic evolution.

Experimental and Computational Details

Aluminophosphate Framework Synthesis. The hydrothermal synthesis of $AlPO_4$-18 was performed according to the procedure established by Simmen et al.,[41] with the aluminum and phosphorus sources being pseudo-boehmite (Catapal-B) and phosphoric acid (85 wt % H_3PO_4), respectively. The organic template agent used was tetraethylammonium hydroxide (TEAOH). The alumina and phosphoric acid were combined with water and subjected to vigorous agitation for 15 min. An aqueous solution of concentrated HCl and TEAOH was then added to the alumina/phosphoric acid mixture. The resulting slurry was stirred for 2 h, producing a viscous white gel with a molar ratio of 0.33 HCl:0.67 $(TEA)_2O$:1.0 Al_2O_3:1.0 P_2O_5:35 H_2O.

A small fraction of the gel was air-dried, and this portion is subsequently referred to as the initial gel without heating, or the zero hour sample. The remainder of the gel was distributed into several Teflon-lined acid digestion bombs and heated in an oven at 150 °C. The autoclaves were quenched in cold water after the specified lengths of heating (1, 2, 6, 24, 60, and 72 h), and the liquid phase of each digestion bomb was separated from the solid phase by centrifugation. The solid materials were then dried in air at room temperature and then calcined as previously described for $AlPO_4$-18.[59] Briefly summarized, a small portion (∼1 g) of each solid was placed in a Tammann crucible and heated at 500 °C for 24 h in order to remove any loosely bound constituents and template molecules within the aluminophosphate frameworks. Powder XRD was used to confirm that the frameworks were unaffected by the calcination process.

Hyperpolarized ^{129}Xe NMR Experiments. The hyperpolarized ^{129}Xe was produced using a home-built optical pumping apparatus with a 60-W dual diode laser (Coherent, Inc.) operating at approximately 80% of maximum power.[60−62] A mixture of 1% xenon gas in a 98% helium and 1% nitrogen buffer gas mixture was used in all experiments, ensuring only low xenon occupancies within the porous frameworks. Nuclear spin hyperpolarization of the xenon gas was achieved by first optically pumping gaseous atomic Rb followed by electron−nuclear spin-exchange that results in ^{129}Xe nuclear spin polarizations of 10% or greater, corresponding to an enhancement of approximately 10^4 over the conventional thermal nuclear spin polarization that takes place in a magnetic field of 4.7 T. All ^{129}Xe NMR spectra were acquired using a Chemagnetics CMX 200 spectrometer operating at a ^{1}H frequency of 200.148 MHz and a ^{129}Xe frequency of 55.365 MHz ($B_0 = 4.7$ T). Chemical shifts were referenced with respect to the ^{129}Xe gas peak ($\delta = 0$ ppm), corrected to the zero-density limit.[63] Bloch-decay spectra were acquired using $\pi/2$ pulses with a duration of 2.2 μs and a recycle delay of 0.5 s. The resulting spectra were scaled according to the weight of the sample in each experiment so that the integrated intensities could be compared from sample to sample. The effects of xenon exchange on the ^{129}Xe NMR spectra

(27) Wilson, S. T.; Lok, B. M.; Messina, C. A.; Cannan, T. R.; Flanigen E. M. *J. Am. Chem. Soc.* **1982**, *104*, 1146.
(28) Wilson, S. T.; Lok, B. M.; Flanigen, E. M. U.S. Patent 4,310,440, 1982.
(29) Flanigen, E. M.; Lok, B. M.; Patton, R. L.; Wilson, S. T. *Pure Appl. Chem.* **1986**, *58*, 1351.
(30) Davis, M. E. *Nature* **2002**, *417*, 813.
(31) Baur, W. H.; Joswig, W.; Kassner, D.; Kornatowski, J. *Acta Crystallogr.* **1994**, B*50*, 290.
(32) Finger, G.; Kornatowski, J.; Jancke, K.; Matschat, R.; Baur, W. H. *Micorporous Mesoporous Mater.* **1999**, *33*, 127.
(33) Prakash, A. M.; Kevan, L.; Zahedi-Niaki, M. H.; Kaliaguine, S. *J. Phys. Chem. B* **1999**, *103*, 831.
(34) Kikhtyanin, O. V.; Vogel, R. F.; Kibby, T. V.; Harris, T. V.; Ione, K. G.; O'Rear, D. J. In *Proceedings of the 12th International Zeolite Conference*; Treacy, M. M. J., Marcus, B. K., Bisher, M. E., Higgins, J. B., Eds.; Materials Research Society: Warrendale, 1999; Vol. 3, p 1743.
(35) Venkatathri, N.; Hegde, S. G.; Sivasanker, S. *J. Chem. Soc. Chem. Commun.* **1995**, 151.
(36) Umamaheswari, V.; Kannan, C.; Arabindoo, B.; Palanichamy, M.; Murugesan, V. *Proc. Indian Acad. Sci. (Chem. Sci.)* **2000**, *112*, 439.
(37) Tušar, N. N.; Mali, G.; Arčon, I.; Kaučič, V.; Ghanbari-Siahkali, A.; Dwyer, J. *Microporous Mesoporous Mater.* **2002**, *55*, 203.
(38) Huang, Y.; Demko, B. A.; Kirby, C. W. *Chem. Mater.* **2003**, *15*, 2437.
(39) Bennett, J. M.; Cohen, J. P.; Flanigen, E. M.; Pluth, J. J.; Smith, J. V. *ACS Symp. Ser.* **1983**, *218*, 109.
(40) *Atlas of Zeolite Framework Type*, 5th ed.; Baerlocher, Ch., Meier, W. M., Olson, D. H., Eds.; Elsevier: Amsterdam, 2001.
(41) Simmen, A.; McCusker, L. B.; Baerlocher, Ch.; Meier, W. M. *Zeolites* **1991**, *11*, 654.
(42) Ratcliffe, C. I. *Annu. Rep. NMR Spectrosc.* **1998**, *36*, 123.
(43) Bonardet, J. L.; Fraissard, J.; Gédéon, A.; Spinguel-Huet, M. A. *Catal. Rev.-Sci. Eng.* **1999**, *41*, 115.
(44) Raftery, D.; Chmelka, B. F. *NMR Basic Principles Progr.* **1994**, *30*, 111.
(45) Goodson, B. M. *J. Magn. Reson.* **2002**, *155*, 157.
(46) Larsen, R. G.; Shore, J.; Schmidt-Rohr, K.; Emsley, L.; Pines, A.; Janicke, M.; Chmelka, B. F. *Chem. Phys. Lett.* **1993**, *214*, 220.
(47) Chen, Q. J.; Fraissard, J. *J. Phys. Chem.* **1992**, *96*, 1814.
(48) Jameson, A. K.; Jameson, C. J.; Gerald, R. E., II *J. Chem. Phys.* **1994**, *101*, 1775.
(49) Ripmeester, J. A.; Ratcliffe, C. I. *J. Phys. Chem.* **1995**, *99*, 619.
(50) Koskela, T.; Ylihautala, M.; Jokisaari, J. *Microporous Mesoporous Mater.* **2001**, *46*, 99.
(51) Nossov, A.; Guenneau, F.; Springuel-Huet, M. A.; Haddad, E.; Montouillout, V.; Knott, B.; Engelke, F.; Fernandez, C.; Gédéon, A. *Phys. Chem. Chem. Phys.* **2003**, *5*, 4479.
(52) Koskela, T.; Jokisaari, J.; Satyanarayana, C. *Micorpor. Mesopor. Mater.* **2004**, *67*, 113.
(53) Chen, Q. J.; Fraissard, J.; Cauffriez, H.; Guth, J. L. *Zeolites* **1991**, *11*, 534.
(54) Chen, Q. J.; Springuel-Huet, M. A.; Fraissard, J. *Chem. Phys. Lett.* **1989**, *159*, 117.
(55) Sholl, D. S.; Lee, C. K. *J. Chem. Phys.* **2000**, *112*, 817.
(56) Sholl, D. S.; Fichthorn, K. A. *J. Chem. Phys.* **1997**, *107*, 4384.
(57) Springuel-Huet, M. A.; Fraissard, J. *J Chem. Phys.* **1989**, *154*, 299.
(58) Davis, M. E.; Saldarriaga, C.; Montes, C.; Hanson, B. E. *J. Phys. Chem.* **1988**, *92*, 2557.
(59) He, H.; Klinowski, J. *J. Phys. Chem.* **1993**, *97*, 10385.
(60) Driehuyh, B.; Cates, G. D.; Miron, E.; Sauer, K.; Walter, D. K.; Happer, W. *Appl. Phys. Lett.* **1996**, *69*, 1668.
(61) Walker, T. G.; Happer, W. *Rev. Mod. Phys.* **1997**, *69*, 629.
(62) Moudrakovski, I. L.; Lang, S.; Ratcliffe, C. I.; Simard, B.; Santyr, G.; Ripmeester, J. A. *J. Magn. Reson.* **2000**, *144*, 372.
(63) Jameson, C. J.; Jameson, A. K.; Cohen, S. M. *J. Phys. Chem.* **1973**, *59*, 4540.

were assessed by comparing the line widths of the peaks corresponding to xenon adsorbed in pure $AlPO_4$-18 and in $AlPO_4$-18 in the 24 h sample. For xenon adsorbed in the $AlPO_4$-18 of the 24 h sample, the ^{129}Xe NMR half-height line width measured was 40 Hz greater than that measured for xenon adsorbed in pure $AlPO_4$-18. Given that the NMR line width of the ^{129}Xe peak arising from xenon adsorbed in pure $AlPO_4$-18 is 240 Hz, exchange broadening of the ^{129}Xe NMR spectra acquired under the experimental conditions used in this study is minimal.

2D-EXSY experiments were performed using hyperpolarized ^{129}Xe NMR. The $\pi/2-\tau_1-\pi/2-\tau_{mix}-\pi/2$ pulse sequence of Ernst[64,65] was employed using a hypercomplex phase cycle.[66−68] Spectra were acquired using mixing times, τ_{mix}, of 1, 5, and 10 ms for the sample that had reacted for 24 h. Each 2D spectrum was acquired with 128 points in the t_1 dimension and 1024 points in the t_2 dimension. The spectra were zero-filled to 1024 points in the t_1 dimension, processed with 100 Hz of line broadening, and symmetrized to overcome distortions from t_1 noise.[69]

Grand Canonical Monte Carlo Simulations. Simulations of the average isotropic ^{129}Xe NMR chemical shifts were first reported for xenon adsorbed in the aluminosilicate NaA.[70,71] The development of the dimer-tensor model,[72,73] implemented within the GCMC scheme, has proven successful in the simulation of anisotropic ^{129}Xe NMR line shapes of xenon adsorbed in various anisotropic environments.[73−77] GCMC simulations have been used as an interpretive tool, providing the correct trends of the ^{129}Xe NMR chemical shift tensors of adsorbed xenon gas. For example, in the two dipeptide nanochannels L-Val-L-Ala and L-Ala-L-Val, the ^{129}Xe NMR line shapes as a function of xenon loading in the two channels were reproduced, as well as the relative magnitudes of the observed chemical shifts of xenon adsorbed in the two different channels.[77] In addition to the simulated ^{129}Xe NMR line shapes, the GCMC computations provide one-body distributions that give detailed information as to the exact shape of the pore accessible to the adsorbed xenon.

The GCMC technique has been thoroughly described by Allen and Tildesly,[78] and the specific implementation of calculating the average xenon NMR chemical shifts was described by Jameson et al.[70,71] The calculations for the present study were preformed using 3D periodic boundary conditions[78] on simulation boxes comprised of $2 \times 2 \times 3$ unit cells of the two different aluminophosphate crystal structures as determined by a Rietveld refinement of X-ray diffraction data.[39,40] The GCMC scheme in this study used Mezei cavity-biased sampling[79] in addition to the standard Norman−Filinov method,[80] to ensure efficient exploration of configuration space.

The potentials used in this study were taken directly from Jameson and are of the Maitland−Smith functional form

$$V = \epsilon\{(6/(n-6))\check{r}^{-n} - (n/(n-6))\check{r}^{-6}\} \quad (1)$$

where n is allowed to vary according to $n = m + \gamma(\check{r} - 1)$, with $\check{r} = r/r_{min}$. The parameters used for the Xe−O potential were $r_{min} = 3.8614$ Å, $\epsilon = 188.63$ K, $\gamma = 8.0$, and $m = 13.0$ and for the Xe−Xe potential $r_{min} = 4.3627$ Å, $\epsilon = 282.29$ K, $\gamma = 11.0$, and $m = 13.0$.[73] The Xe−Xe potential parameters are a fit to the Aziz−Slaman empirical potential.[81]

The dimer-tensor model was previously implemented in simulations of ^{129}Xe NMR line shapes of xenon in the aluminophosphate $AlPO_4$-11.[73] Briefly, in the dimer-tensor model, the total intermolecular ^{129}Xe shielding tensor is assumed to be the pairwise additive sum of the xenon shielding tensors of all Xe−O and Xe−Xe dimmers, corresponding to the interaction of a particular xenon with all oxygen atoms comprising the framework and other xenon atoms present within the framework. It is assumed that the perpendicular and parallel components of the Xe−O symmetric shielding tensor are well behaved functions of internuclear separation. Under this assumption, the six unique components of the symmetric xenon shielding tensor in the Cartesian frame of the simulation box can be calculated for any arbitrary configuration of xenon atoms within the box. The relationship of the dimer tensor components to the *xx*, *xy*, etc. components of the total ^{129}Xe shielding tensor was derived by Jameson.[71,73] The shielding tensor functions for the Xe−O dimers of xenon adsorbed in $AlPO_4$-11 are given elsewhere[73] and were obtained from a fit to ab initio calculations of the Xe−Ar dimer at varying r_{Xe-Ar}. The resulting shielding tensor functions were then scaled according to the methods prescribed by Jameson et al.[82,83] Similarly, the Xe−Xe shielding tensor functions are also known from quantum mechanical calculations.[85] The simulated line shape results from the projections of the total ^{129}Xe shielding tensor being binned into a histogram for various orientations of the static magnetic field, B_0, with respect to the Cartesian coordinate frame of the simulation box. The interested reader will find a detailed description of the dimer-tensor model in the Supporting Information.

Results and Discussion

Following the Formation of $AlPO_4$-5 and $AlPO_4$-18 using Hyperpolarized ^{129}Xe NMR. One-dimensional ^{129}Xe NMR spectra of gaseous hyperpolarized xenon in seven different $AlPO_4$ preparations, at varying reaction times, are shown in Figure 3. The hyperpolarized ^{129}Xe NMR spectrum acquired for the unheated sample (0 h), consisting of the starting materials, shows a broad peak at 7 ppm in addition to the gas peak (see Figure 3a). The crystallinity of this sample was confirmed by XRD, which is consistent with another investigation.[38] The small ^{129}Xe chemical shift observed is assigned to xenon adsorbed in the intercrystallite space of the starting materials.[84]

(64) Jeener, J.; Meier, B. H.; Bachmann, P.; Ernst, R. R. *J. Chem. Phys.* **1979**, *71*, 4546.
(65) Ernst, R. R.; Bodenhausen, G.; Wokaun, A. *Principles of Nuclear Magnetic Resonance in One and Two Dimensions*; Oxford: Oxford, 1987; Chapter 9.
(66) Bax, A.; Marion, D. J. *J. Magn. Reson.* **1988**, *78*, 186.
(67) Furihata, K.; Ohuchi, M.; Seto, H. *Tetrahedron Lett.* **1987**, *28*, 3353.
(68) States, D. J.; Haberkorn, R. A.; Ruben, D. J. *J. Magn. Reson.* **1982**, *48*, 286.
(69) Hull, W. E. In *Two-Dimensional NMR Spectroscopy: Applications for Chemists and Biochemists*, 2nd ed.; Croasmun, W. R., Carlson, R. M. K., Eds.; VCH Publishers: New York, 1994; p 67.
(70) Jameson, C. J.; Jameson, A. K.; Baello, B. I.; Lim, H. M. *J. Chem. Phys.* **1994**, *100*, 5965.
(71) Jameson, C. J.; Jameson, A. K.; Lim, H. M.; Baello, B. I. *J. Chem. Phys.* **1994**, *100*, 5977.
(72) Jameson, C. J.; de Dios, A. C. *J. Chem. Phys.* **2002**, *116*, 3805.
(73) Jameson, C. J. *J. Chem. Phys.* **2002**, *116*, 8912.
(74) Jameson, C. J. *J. Am. Chem. Soc.* **2004**, *126*, 10450.
(75) Stueber, D.; Jameson, C. J. *J. Chem. Phys.* **2004**, *120*, 1560.
(76) Jameson, C. J.; Stueber, D. *J. Chem. Phys.* **2004**, *120*, 10200.
(77) Moudrakovski, I.; Soldatov, D. V.; Ripmeester, J. A.; Sears, D. N.; Jameson, C. J. *Proc. Natl. Acad. Sci. U.S.A.* **2004**, *101*, 17924.
(78) Allen, M. P.; Tildesley, D. J. *Computer Simulation of Liquids*; Oxford: Oxford, 1987.
(79) Mezei, M. *Mol. Phys.* **1980**, *40*, 901.
(80) Norman, G. E.; Filinov, V. S. *Hight Temp. USSR* **1969**, *7*, 216.
(81) Aziz, R. A.; Slaman, M. J. *Mol. Phys.* **1986**, *57*, 825.
(82) Jameson, C. J.; de Dios, A. C. *J. Chem. Phys.* **1993**, *98*, 2208.
(83) Jameson, C. J.; Sears, D. N.; de Dios, A. C. *J. Chem. Phys.* **2003**, *118*, 2575.
(84) Moudrakovski, I. L.; Nossov, A.; Lang, S.; Breeze, S. R.; Ratcliffe, C. I.; Simard, B.; Santry, G.; Ripmeester, J. A. *Chem. Mater.* **2000**, *12*, 1181.
(85) Sears, D. R.; Klug, H. P. *J. Chem. Phys.* **1962**, *37*, 3002.

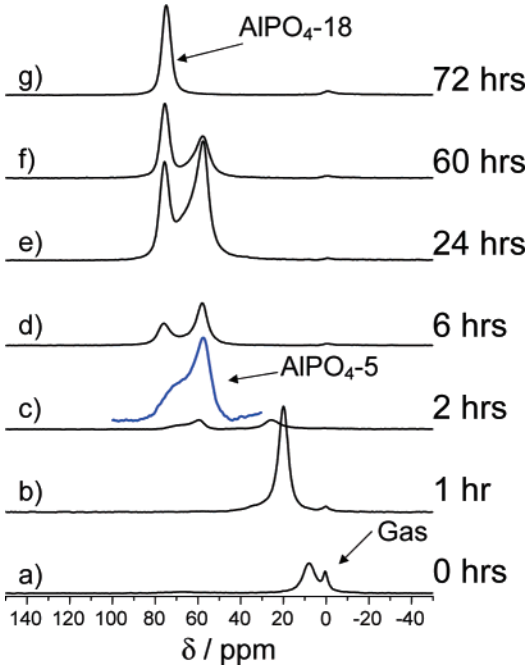

Figure 3. ^{129}Xe NMR spectra of hyperpolarized xenon in calcined aluminophosphate samples after various heating times. The inset in c is an expansion (10× vertical magnification) of the peak centered at $\delta_{iso} \approx 63$ ppm.

The ^{129}Xe NMR spectrum of the product obtained after 1 h of heating is shown in Figure 3b. Powder XRD confirms an amorphous structure, in agreement with previous work.[38] The peak observed in the ^{129}Xe NMR spectrum near 23 ppm suggests that the sample possesses voids that are occupied by xenon. The isotropic line shape of the peak as well as its chemical shift indicates that the voids in the sample lack organization and that the void dimensions are in the mesoporous regime (2−50 nm), respectively.[43]

The third spectrum, shown in Figure 3c, corresponds to the preparation that was heated at 150 °C for 2 h. The ^{129}Xe NMR peak at 63 ppm is characteristic of xenon confined to the pores of $AlPO_4$-5.[50,52,53] The observed ^{129}Xe NMR line shape of xenon inside $AlPO_4$-5 is in agreement with the spectrum recently reported by Jokisaari and co-workers[52] in their investigation of the pressure dependence of the ^{129}Xe NMR line shape of xenon in $AlPO_4$-5. Additionally, Ripmeester and co-workers have studied xenon adsorbed in SSZ-24, an aluminosilicate that is isostructural with $AlPO_4$-5, and report a ^{129}Xe NMR line shape very similar to that observed for xenon in $AlPO_4$-5.[84] The ^{129}Xe NMR spectrum in Figure 3c is complemented by the XRD pattern, which indicates that the reaction product contains a small amount of the AFI structural type. Unlike the ^{129}Xe NMR peak from the sample heated for 1 h, the $AlPO_4$-5 peak shows a well-defined anisotropic line shape (blue inset in Figure 3). The observation of an anisotropic ^{129}Xe NMR line shape is expected, since the $AlPO_4$-5 framework has an axially symmetric one-dimensional channel that is approximately 7.3 Å in diameter.[39] Given that the van der Waals diameter of xenon is approximately 4.4 Å,[85] one can expect that the xenon atoms adsorbed within the channels of $AlPO_4$-5 will be found in configurations where only one xenon atom resides in a single plane perpendicular to the channel axis. The xenon chemical shift tensor components perpendicular to the channel axis (57 ppm) are slightly more shielded than the chemical shift tensor component parallel to the channel axis (74 ppm).

The fourth spectrum, shown in Figure 3d, was acquired with reaction products that had been heated for 6 h. The spectrum has a peak near 74 ppm, in addition to the line shape already assigned to xenon within $AlPO_4$-5. The powder XRD pattern indicates that this sample contains both AFI and AEI framework types, corresponding to $AlPO_4$-5 and $AlPO_4$-18, respectively. Therefore, we attribute the peak at 74 ppm to xenon residing in $AlPO_4$-18. The peak shows no obvious anisotropic line shape, indicating that the xenon chemical shift anisotropy is small, less than 3 ppm. This is attributed to the fact that $AlPO_4$-18 possesses a three-dimensional pore system where the intersections of the pores form an asymmetric pear-shaped cage.[41] While the cage is not perfectly spherical, the asymmetry does not produce observable variations in the components of the ^{129}Xe magnetic shielding tensor, because the xenon atoms adsorbed in $AlPO_4$-18 average over the entire internal volumes of the occupied cages during the course of the NMR experiment. This observation is supported by theoretical simulations (vide infra).

Of the samples investigated, the ^{129}Xe NMR peak from xenon in the $AlPO_4$-5 framework reaches a maximum integrated intensity for the preparation quenched after 24 h of heating (see Figure 3e). For reactions carried out longer than 24 h, the ^{129}Xe NMR spectra indicate that the amount of $AlPO_4$-5 present in the mixture decreases as $AlPO_4$-5 is converted to $AlPO_4$-18. The intensity of the ^{129}Xe NMR peak of xenon in $AlPO_4$-18 also increases in the series of reaction products from 6 h onward, reaching a maximum intensity at 72 h of heating, at which time all the $AlPO_4$-5 has been converted to $AlPO_4$-18.

The ^{129}Xe NMR results shown in Figure 3 demonstrate that the pore structure of the aluminophosphate undergoes the same transformations that have been observed using powder XRD and solid-state ^{31}P and ^{27}Al NMR.[38] The ^{129}Xe NMR spectra indicate that, in the sample that was unheated, the xenon initially resides in the interstitial space. In the preparation heated for 1 h, the xenon occupies large disordered voids present in the amorphous domains of this sample. The formation of $AlPO_4$-5, which begins to occur after approximately 2 h of heating, provides a one-dimensional cylindrical channel in which xenon is readily adsorbed, giving rise to the observed axially symmetric ^{129}Xe NMR line shape. Finally, after reacting for approximately 6 h, $AlPO_4$-18 begins to form and continues to form until, after 72 h of heating, only $AlPO_4$-18 is present.

GCMC Simulations of ^{129}Xe NMR Line Shapes. To provide a theoretical description of the observed ^{129}Xe NMR line shapes, GCMC simulations were carried out separately for xenon adsorbed in $AlPO_4$-5 and $AlPO_4$-18. Since the measurements of the $AlPO_4$-5 and $AlPO_4$-18 ^{129}Xe NMR line shapes were carried out with both aluminophosphates in the same sample under identical experimental conditions (1% Xe gas, 98% He gas, and 1% N_2 gas), the simulations of xenon in $AlPO_4$-5 and $AlPO_4$-18 were likewise carried out under identical conditions, using the same chemical potentials and temperatures. The chemical potential used in the GCMC

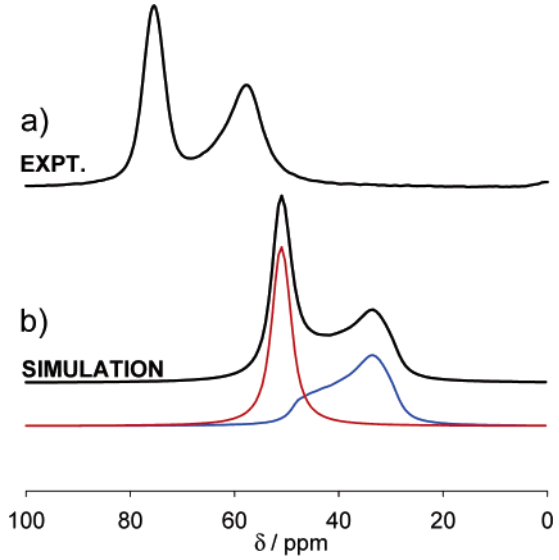

Figure 4. (a) Experimental spectrum was acquired after 60 h of sample heating. (b) GCMC-simulated ^{129}Xe NMR line shapes of xenon in $AlPO_4$-5 (blue) and $AlPO_4$-18 (red).

runs corresponded to low xenon occupancy, similar to experimental conditions. The GCMC simulations were carried out at a temperature of 300 K, close to the temperature at which the ^{129}Xe NMR measurements were performed. It should be pointed out that, by carrying out separate simulations of xenon adsorbed in $AlPO_4$-5 and $AlPO_4$-18, the effects of exchange on the spectrum are completely neglected. However, as already discussed, exchange broadening is nominal under the experimental conditions used in this study.

A comparison of the experimental spectrum with the simulated line shapes is shown in Figure 4. As can be seen in Figure 4b, the simulated ^{129}Xe NMR line shape resulting from xenon in $AlPO_4$-18 has very little anisotropy (red line), whereas the simulations of xenon adsorbed in $AlPO_4$-5 has a distinct anisotropic line shape (blue line) with a span of 13 ppm. The total simulated line shape shown in Figure 4b (black line) compares well with the experimental spectrum shown in Figure 4a. The relative integrated intensities of the ^{129}Xe NMR peaks in the experimental spectrum provide a measure of the relative amounts of $AlPO_4$-5 and $AlPO_4$-18 present in the sample. In the simulation of the total line shape, the amounts of $AlPO_4$-5 and $AlPO_4$-18 were assumed to be equal. The results of the simulations indicate that the sample heated for 60 h has approximately equal fractions of $AlPO_4$-5 and $AlPO_4$-18.

The one-body distribution for xenon adsorbed in $AlPO_4$-5 reveals a distinct axial symmetry of the configurations of xenon within the channel of $AlPO_4$-5 (see Figure 5). As can be seen from the one-body distribution plotted perpendicular to the channel axis (Figure 5a), the xenon resides in a trough near the channel walls, rarely sampling configurations at the center of the channel. The distribution parallel to the channel axis (Figure 5b), shows that the xenon averages over discrete areas corresponding to the faces of the six-member rings formed by the aluminum and phosphorus atoms in the channel wall. This is analogous to previous simulations of xenon in SSZ-24.[74]

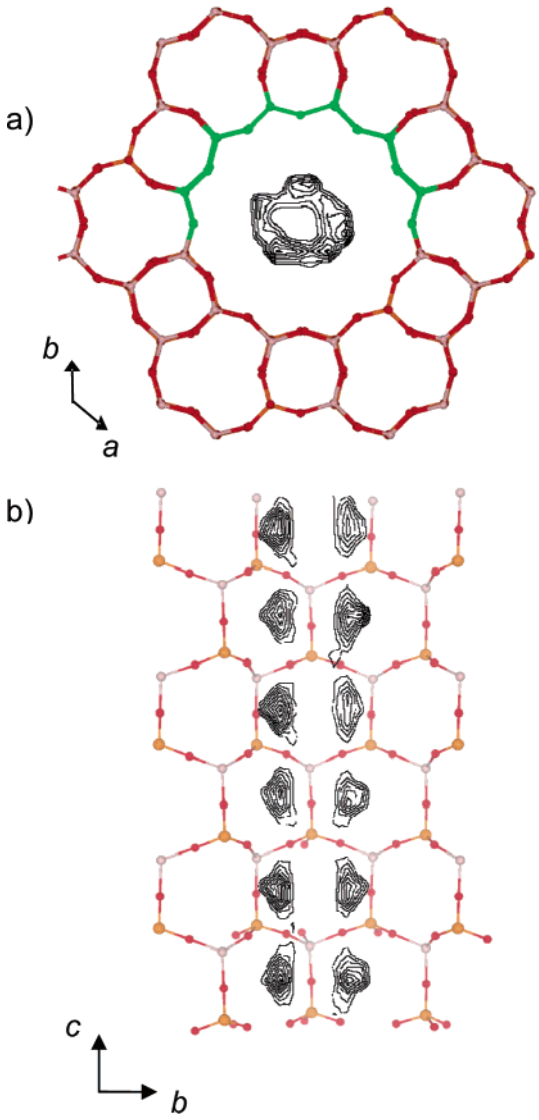

Figure 5. One-body distribution of xenon in $AlPO_4$-5 at 300 K and low xenon occupancy: (a) in a plane perpendicular to the crystal *c*-axis and (b) in a plane parallel to the channel axis along the crystal *c*-axis. The structure of $AlPO_4$-5 has been overlaid for reference. The atoms colored green in panel (a) represent the channel wall atoms depicted in panel (b).

Examination of the one-body distribution of xenon adsorbed in $AlPO_4$-18 obtained from the GCMC simulations is shown in Figure 6. In the low-loading limit, the xenon is only found in the cages formed at the pore intersections. The contours shown in Figure 6a represent the density of configurations sampled during the GCMC simulation in a plane perpendicular to the *c*-axis of the crystal, 3.85 Å from the front edge of the supercell shown in Figure 2. Figure 6a also shows the asymmetry of the cage depicted by the higher density of sampled configurations in the lower half of the cage. The shape of the one-body distribution in the selected plane is in accord with the "pear-shape" description of the cage.[41] When viewed along the *a*-axis of the simulation box (Figure 6b), the one-body distribution reflects the alternation of asymmetric cages along the *c*-axis. This view clearly shows that the distribution depicted in Figure 6a was taken from a plane perpendicular to the one shown in Figure 6b with the bulbous portion of the pear-shaped distribution at the bottom of the cage. Despite the asymmetry in these cages, the xenon atom sufficiently averages over all configurations

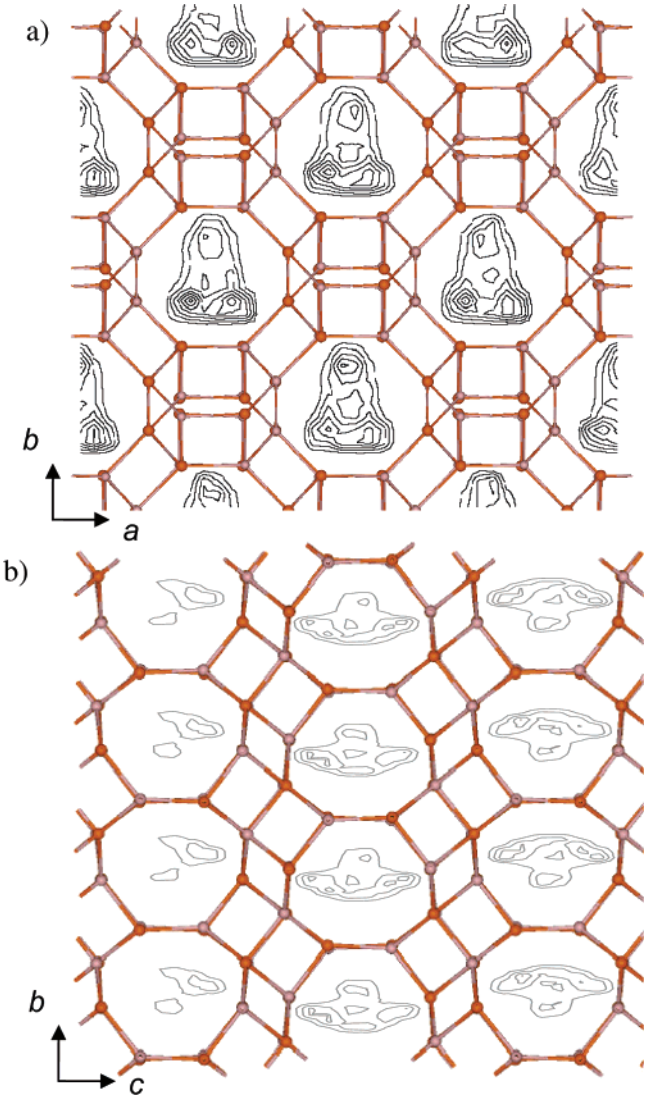

Figure 6. One-body distribution of xenon in $AlPO_4$-18 at 300 K and low xenon occupancy. (a) The plotted distribution is viewed down the *c*-axis of the crystal. The structure of $AlPO_4$-18 in the *ab* plane of the crystal has been overlaid for reference. (b) The one-body distribution as viewed down the *a*-axis of the crystal. The structure of $AlPO_4$-18 in the *bc* plane of the crystal has been overlaid for reference.

within the cage during the time of the experiment to result in a line shape with a small chemical shift anisotropy of approximately 2 ppm.

It is important to point out that the simulated line shapes in Figure 4 are not a fit of the experimental spectrum; no adjustable parameters were used; thus, it is not surprising that the magnitudes of the isotropic chemical shifts and the respective spans of the line shapes deviate from experiment. These deviations are due to the fact that the potential functions and the dimer-tensor shielding functions used were taken directly from simulations of xenon adsorbed in $AlPO_4$-11.[73] The nuclear magnetic shielding tensor functions used for $AlPO_4$-11 were obtained by scaling the Xe−Ar dimer-tensor shielding functions to a set of Xe−O dimer-tensor shielding functions. The same potentials used in this study were previously used for the study of xenon in 1:1 aluminosilicate zeolites.[70,71] The simulations are used as an interpretive tool reproducing the correct trends for the ^{129}Xe chemical shift tensors for xenon adsorbed in the two different frameworks. To obtain more quantitative agreement with

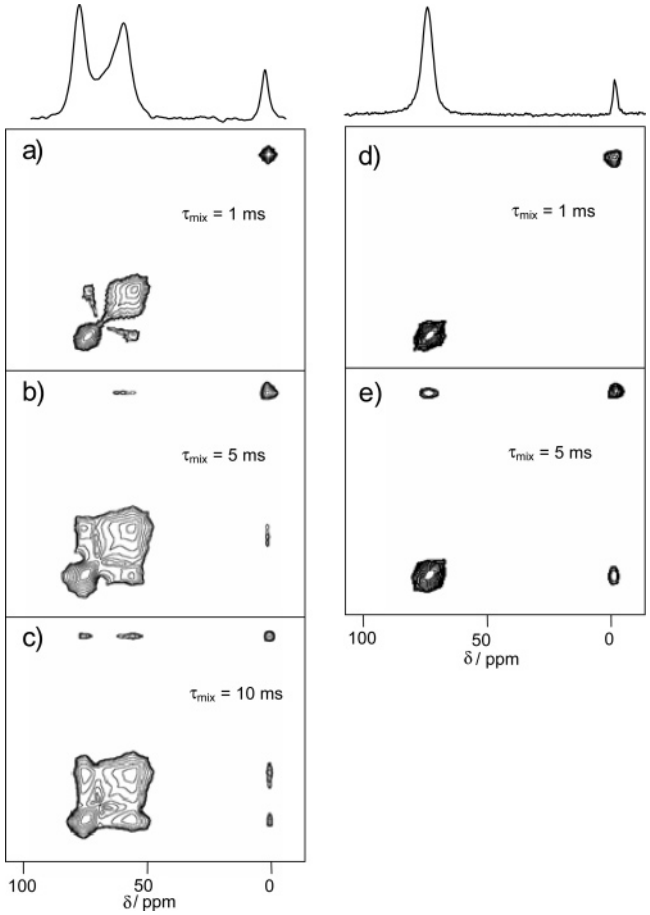

Figure 7. Left column, ^{129}Xe 2D-EXSY spectra of the sample heated for 24 h at three different mixing times: (a) $\tau_{mix} = 1$ ms, (b) $\tau_{mix} = 5$ ms, and (c) $\tau_{mix} = 10$ ms. The corresponding 1D spectrum collected at the same time as the 2D-EXSY spectra were acquired (32 scans) is shown at the top. Right column, the ^{129}Xe 2D-EXSY spectra of xenon adsorbed in pure $AlPO_4$-18 at two different mixing times: (d) $\tau_{mix} = 1$ ms and (e) $\tau_{mix} = 5$ ms.

experiment, further refinement of both the dimer-tensor shielding functions and potential functions is necessary to optimize them for specific use in the study of aluminophosphates.

2D ^{129}Xe NMR Study of Xenon Dynamics. To provide insight into the pore interconnectivity and xenon dynamics, 2D-EXSY experiments were performed on the preparation heated for 24 h (see Figure 3e). The resulting 2D-spectra acquired with three different τ_{mix} times are shown in Figure 7a−c. The cross-peaks indicate an exchange of xenon atoms between the corresponding environments on the diagonal within the period of τ_{mix}.[64,65] Figure 7a shows a 2D-EXSY spectrum acquired with $\tau_{mix} = 1$ ms. The presence of cross-peaks between the two ^{129}Xe NMR peaks assigned to xenon in $AlPO_4$-5 and $AlPO_4$-18 suggests that on a time scale of 1 ms the exchange of xenon between these environments occurs rapidly. On the other hand, the absence of cross-peaks between the xenon peak assigned to the bulk xenon gas and xenon in either $AlPO_4$-5 or $AlPO_4$-18 suggests that the xenon exchange is slow. The 2D-EXSY spectrum in Figure 7b, acquired with $\tau_{mix} = 5$ ms, shows the xenon exchange between the aluminophosphate environments as well as a small cross-peak between xenon in the $AlPO_4$-5 and the free xenon gas. The presence of this latter cross-peak indicates that xenon in $AlPO_4$-5 exchanges with the bulk xenon gas

on a 5 ms time scale. However, on the same time scale, the xenon adsorbed in $AlPO_4$-18 shows no evidence of exchange with the bulk gas. The 2D-EXSY spectrum in Figure 7c was acquired with $\tau_{mix} = 10$ ms and demonstrates that on this time scale the xenon gas exchanges among all three environments.

The 2D-EXSY results for the pure $AlPO_4$-18, shown in Figure 7d,e, indicate that exchange between the xenon adsorbed in $AlPO_4$-18 and the free gas occurs on a time scale of 5 ms. Therefore, the fact that there is no exchange peak between the xenon adsorbed in $AlPO_4$-18 and the free gas in the 5 ms 2D-EXSY spectrum of the mixture of reaction products (Figure 7b) indicates that the rate of exchange between xenon in $AlPO_4$-18 and the free gas is hindered by the presence of $AlPO_4$-5.

Conclusions

Hyperpolarized ^{129}Xe NMR spectroscopy has been shown to be an effective method for monitoring the formation of microporous $AlPO_4$-5 and $AlPO_4$-18, allowing for the inspection of the porosity of the aluminophosphate frameworks as they are formed. The results indicate that, first, an amorphous environment possessing irregular voids is formed, then the $AlPO_4$-5 framework is formed, and finally, $AlPO_4$-5 is transformed into $AlPO_4$-18. The unique porous environments of the aluminophosphate frameworks present at various stages of the $AlPO_4$-18 synthesis give rise to signature ^{129}Xe NMR line shapes, permitting the characterization of porosity during the synthetic process. For a mixture of $AlPO_4$-5 and $AlPO_4$-18, GCMC simulations of the ^{129}Xe NMR line shapes compare favorably with experiment and provide detailed information about the distribution of xenon atoms within the pores. The use of 2D-EXSY NMR experiments has indicated that the two domains of $AlPO_4$-5 and $AlPO_4$-18 present after an intermediate reaction time are in close contact and that the presence of the mixture of framework types results in complex exchange between the three different environments. This finding supports the conclusions of Huang et al.[38] that the $AlPO_4$-18 framework evolves from the $AlPO_4$-5 structure. Most important, the research reported here demonstrates the utility of ^{129}Xe NMR spectroscopy combined with GCMC simulations in the study of framework formations during the synthesis of microporous materials. The sensitivity of the ^{129}Xe magnetic shielding tensor to its local environment makes hyperpolarized ^{129}Xe NMR spectroscopy an ideal method for the discrimination of multiple frameworks formed in a single reaction mixture. Clearly, it should be possible to extend the approach taken here to investigate the formation of other porous frameworks, such as the silicon-doped aluminophosphate SAPO-44.[86]

Acknowledgment. We thank the Natural Sciences and Engineering Council of Canada, the Alberta Ingenuity Fund, and the University of Alberta for research grants and scholarships. D.N.S. is an Izaak Walton Killam Postdoctoral Fellow and R.E.W. is a Canada Research Chair in Physical Chemistry at the University of Alberta. The authors wish to thank Prof. C. J. Jameson at the University of Illinois at Chicago for graciously providing the GCMC simulation code and for helpful discussions. We acknowledge Prof. A. Mar at the University of Alberta, for use of his high-temperature ovens, and Dr. Stephen Lang, Dr. Igor Moudrakovski, and Dr. John Ripmeester of the Steacie Institute for Molecular Sciences, NRC of Canada, for their advice in constructing the continuous flow diode laser system used to produce the hyperpolarized xenon. We thank Prof. Takahiro Ueda, a sabbatical visitor in our lab, for helping construct the continuous flow apparatus.

Supporting Information Available: A detailed description of the dimer-tensor model as implemented within the GCMC simulations is provided. This material is available free of charge via the Internet at http://pubs.acs.org.

CM0513132

(86) Huang, Y.; Machado, D.; Kirby, K. W. *J. Phys. Chem. B* **2004**, *108*, 1855.